Combustion in a horizontal channel partially filled with a porous media

C. Johansen* and G. Ciccarelli
Queen's University, 130 Stuart Street, Kingston, Ontario, Canada K7L 3N6

Contact author email: johansen@ucalgary.ca

Abstract Experiments were carried out to investigate the combustion propagation phenomenon in a horizontal channel partially filled with ceramic-oxide spherical beads. A 1.22 m long, 43 mm nominally thick layer of spherical beads is located at the ignition end of a 2.44 m long, 76 mm square channel. Tests were performed with 6.4 mm and 12.7 mm diameter beads. A flame is ignited at the bead end wall by an automotive spark ignition system. Flame propagation and pressure measurements are obtained via ionization probes and piezoelectric pressure transducers mounted on the top and bottom surfaces of the channel. High-speed schlieren video was used to visualize the structure of the explosion front. Experiments were performed with a 31 percent nitrogen diluted stoichiometric methane-oxygen mixture at room temperature and at an initial pressure in the range of 15 kPa to 50 kPa. For initial pressures of 15 kPa and 20 kPa the flame accelerates to a velocity close to the speed of sound in the combustion products. For initial pressure of 30 kPa and higher DDT occurs in the gap above the bead layer. An explosion front propagating at a velocity just under the CJ detonation velocity is detected in the bead layer even though the bead layer pore size is much smaller than the detonation cell size. It is demonstrated that flame propagation within the bead layer is the driving force behind the very rapid flame acceleration observed, however the DDT event occurring in the gap above the bead layer is not affected by the bead layer porosity. Schlieren video indicates that the structure of the explosion front varies across the channel height and with propagation distance down the channel.

Keywords flames, porous media, explosion

1 Introduction

Flame propagation in porous media has been studied for many years in the context of explosion safety. In the chemical industry porous media is used as an integral part of processes involving combustible gases. Porous media is often used in flame arrester design because it provides a large surface area that can extract energy from the flame, ultimately leading to quenching. The flame quenching limit in a porous media consisting of spherical beads has been defined by a critical Peclet number of roughly 65, where the characteristic length scale and velocity is taken to be the bead diameter and laminar flame speed [1,2]. For conditions where the Peclet number is above the critical value, flame propagation in a loosely packed bed of beads is possible and in general flame acceleration is observed to be stronger than in a tube filled with obstacles [3].

Babkin et al. [4] proposed that different steady-state flame propagation regimes exist in porous media that are characterized by the propagation mechanism and the front velocity. The regimes of interest to this study include “high velocity flames” (0.1-10 m/s), “sound velocity flames” (100-300 m/s), “low velocity detonation” (500-1000 m/s) and “normal detonations” (1500-2000 m/s). Pinaev [5] studied the behavior of flames propagating in porous media over this complete propagation regime. Pinaev noted that for front speeds greater than 5 m/s there is a pressure rise that coincides with the reaction zone, and that the pressure rise associated with the front steepens with increased propagation velocity. Makris et al. [6] showed that for detonation waves propagating in a porous media the measured velocity varies depending on the

average pore size relative to the detonation cell width. They also showed that in order to achieve a Chapman-Jouget (CJ) detonation the pore size must accommodate at least thirteen detonation cells widths [6].

The propagation regimes observed in porous media are analogous to those observed in obstacle laden tubes, i.e., weak flames, choked flames, quasi-detonation, and CJ detonations [7]. For a fuel-oxidizer mixture at a given thermodynamic condition, the geometry governs the flame acceleration and ultimately the steady-state explosion front propagation velocity. In these two geometries, the flow path is characterized by the bead diameter and the obstacle blockage ratio. Both of these flow geometries perturb the unburned gas flow field ahead of the flame. This includes the generation of spatial velocity gradients and the production of turbulence that leads to increased flame surface area and the local burning rate. Both of these effects result in the enhancement of the volumetric burning rate. This produces a feed back loop between the flame and unburned gas flow that leads to flame acceleration. Conversely, compared to an unobstructed duct, these two flow geometries add wall surface area that extracts energy from the reaction front. As a result, the enhanced momentum and heat losses from the explosion front limit the peak velocity.

Experiments investigating flame propagation in porous media are typically carried out in a vertically oriented tube where the cross-section is filled with the media. In this study, a layer of beads is located in the bottom half of a horizontal square cross-section channel, such that a long cavity free of beads exists in the upper part of the channel. This bead free volume will be referred to as the gap here on in. Flame propagation in this geometry is the result of a combination of influences associated with the bead layer and the gap above. For example, the bead layer introduces turbulence in the unburned gas flow within the bead layer and the top of the bead layer provides surface roughness that promotes turbulence within the gap above the bead layer. Both of these factors lead to enhanced flame acceleration in the gap and within the bead layer. The combustion in the gap is more complex then that in a rough surface duct since mass transport across the bead layer top surface is also possible. The combustion front in this unique geometry is tracked by ionization probes and pressure transducers in both the bead layer and the gap above. High-speed photography is used to visualize the structure of the combustion front across the channel height.

2 Experimental Apparatus

Experiments were carried out in a 2.44 m long, 76 mm square horizontal channel partially filled with a layer of loosely packed 12.7 mm, or 6.4 mm, diameter ceramic-oxide beads. The bead layer is 1.22 m long extending from one end wall to a 38 mm high fence-type obstacle located at roughly mid span of the channel. The channel consists of four equal length interchangeable modules.

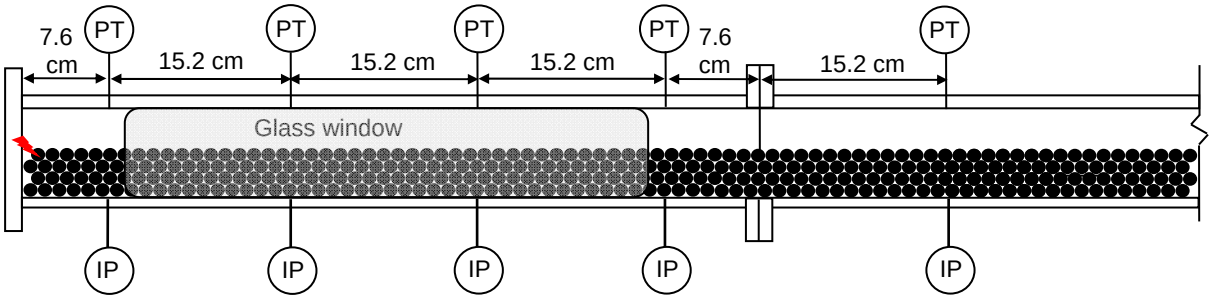

Fig 1 Schematic showing optical channel with instrumentation. *PT* pressure transducer, *IP* ionization probe

In the optical module shown in Fig. 1, 19 mm thick glass panels are integrated into the channel front and back sides to facilitate 444 mm of unobstructed optical access. Visualization of flame propagation in the gap above the bead layer is obtained through a high-speed single-pass schlieren photography system. Schlieren video was obtained using continuous light from a 50 W Xenon lamp. A 254 mm diameter parabolic mirror was used to collimate the light and a second similar mirror was used to focus the beam at a vertical knife edge. The schlieren image was captured by a Photron Fastcam 1024 PCI camera that uses a 1024x1024 pixel CMOS sensor. The maximum speed using the full CMOS sensor is 1000 frames per second and the fastest shutter speed is 1.5 μs. Higher camera speeds are possible if only a sector of the sensor is used.

The optical channel module is equipped with four instrumentation ports spaced 152 mm apart and 76 mm from each end flange on the top and bottom surfaces. The full optical module is shown schematically in Fig.1. Each non-optical module is equipped with two instrumentation ports spaced 305 mm apart and 152 mm from the end flanges on both the top and bottom surfaces. The instrumentation configuration for most of the flame acceleration tests involved four piezoelectric pressure sensors mounted in instrumentation ports on the top surface. Ionization probes were mounted in each remaining instrumentation port on the bottom and top channel surface protruding 15 mm into the test section. In some tests ionization probes were mounted in both the top and bottom channel surfaces at the same axial position allowing for a comparison of flame speed through the porous media and in the gap above.

The channel is filled with a nitrogen diluted stoichiometric methane-oxygen mixture given by $CH_4 + 2(O_2 + 2/3N_2)$. The mixture is produced in a separate mixing chamber by the method of partial pressures. An automotive spark ignition system is used to ignite the flame at the bead layer end of the channel. The spark plug electrode is located at the bead layer surface. Experiments were performed at room temperature at initial pressures in the range of 15 kPa to 50 kPa. The ignition limit for the spark plug ignition system used in the experiments was found to be 14 kPa.

3. Results and Discussion

Some preliminary tests were performed in a vertical 76 mm diameter tube completely filled with the same 12.7 mm ceramic beads in order to characterize the flame propagation phenomenon. Ignition was induced by a spark plug mounted on the top end plate and flame time-of-arrival down the 610 mm long tube was recorded by ionization probes spaced at one tube diameter. The flame velocity inferred from the ionization probe data over the initial pressure range of 15-60 kPa is provided in Fig. 2. For all the tests the flame accelerates very quickly in the first 0.2 m reaching a velocity in the range of 800-1000 m/s by the end of the tube. These velocities are just below the speed of sound in the combustion products, i.e., 1029-1043 m/s for the initial pressure range 20-50 kPa, which represents the upper velocity limit for steady propagating deflagrations. There is a slight deceleration of the flame in the second half of the tube so the final stable velocity could not be measured due to the short length of the tube. As expected, flame acceleration is more pronounced for the more reactive mixtures corresponding to a higher initial pressure. Also the final flame velocity is found to be larger at higher initial pressures due to a reduction in the flame thickness with increased pressure and thus lower heat and momentum losses to the beads. For the test performed at an initial pressure of 60 kPa it appears that DDT occurred but the detonation quickly failed. The calculated CJ detonation velocity for the test mixture at 298K is 2170 m/s. This value does not vary significantly over the initial pressure range tested.

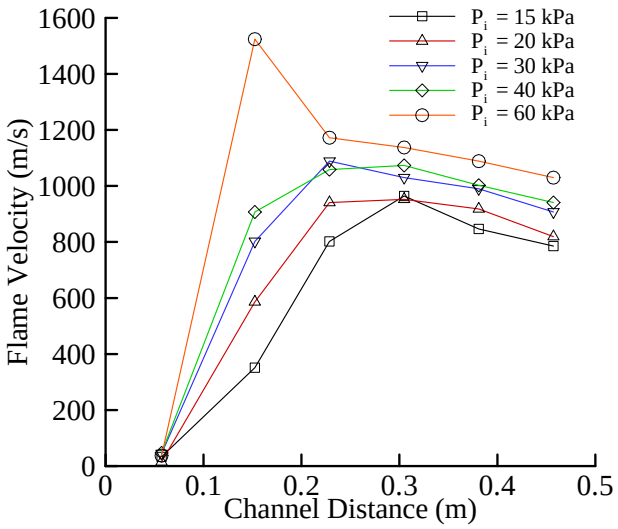

Fig 2 Flame velocity measured down the length of a 76 mm diameter tube completely filled with 12.7 mm beads

Table 1 CJ detonation properties and channel geometric scaling

Initial pressure (kPa)	CJ Velocity (m/s)	CJ Pressure (atm)	λ (mm)	d_{pore}/λ	h_{gap}/λ
20	2124	4.82	~76	~0.02	~0.4
30	2139	7.32	21-31	0.06-0.1	1-1.5
40	2149	9.85	16-21	0.1-0.13	1.5-2
50	2157	12.39	12-16	0.13-0.17	2-2.5

The detonation cell width, λ, for the test mixture over the initial pressure range of interest was measured at the end of the 2.44 m long channel. The cellular structure was found to be irregular, which is common for methane mixtures. The cell size range measured from a single foil at each initial pressure is provided in Table 1. A clear cell size measurement could not be made for the mixture at an initial pressure of 20 kPa, however a detonation propagated in the 76 mm unobstructed channel so the cell size is assumed to be 76 mm. The ratio of the average pore cavity diameter, d_p, and the detonation cell width is provided in Table 1. The average pore cavity diameter for a closely packed bed of spheres is taken to be 0.3 times the bead diameter [8]. Based on the measured cell width data, the bead bed pore size is too small to accommodate a detonation cell for the initial pressure range of 20-50 kPa. This explains why a detonation wave was not observed in the beads over this initial pressure range, see Fig. 2. The same would be expected for the bead layer tests, no detonation is expected through the bead layer.

Bead Layer Tests

For the two bead sizes arranged in a bead layer configuration, the nominal bead layer thickness was approximately 43 mm. The first configuration consisted of four layers of 12.7 mm beads and the second configuration consisted of eight layers of 6.4 mm beads. The flame velocity measured in the gap along the full length of the channel using 12.7 mm beads is shown in Fig. 3a. The data points are the average from four tests and the vertical error bars are the standard deviation. A large range in flame velocities are observed over the initial pressure range tested,

i.e., 15 - 50 kPa. For the least reactive initial mixture condition corresponding to an initial pressure of 15 kPa the flame accelerates to a maximum velocity of 900 m/s at the end of the bead layer, i.e., 1.22 m from the ignition end wall. This velocity is just below the 1020 m/s speed of sound of the combustion products. Once the flame leaves the bead layer section at mid span of the channel the velocity remains relatively constant to the end of the channel. At this initial pressure the cell size is larger than the gap height of 33 mm, see Table 1.

The initial flame acceleration is enhanced as the initial pressure is raised. At an initial pressure of 20 kPa the flame accelerates to the speed of sound of the combustion products in a distance of 0.7 m. The flame velocity remains constant for a short distance and then increases steadily as the flame transitions from the bead layer section to the smooth full channel section. A velocity of roughly 2000 m/s is achieved by the end of the channel. The CJ detonation velocity at this initial pressure is 2124 m/s (see Table 1), which indicates that DDT occurred after the flame left the bead layer section. As was the case for 15 kPa, at 20 kPa the cell size is larger than the gap height and thus DDT above the bead layer is not possible. However, in the second half of the channel the full channel height can accommodate at least a single detonation cell. Most likely detonation initiation occurs when the shock wave preceding the flame diffracts around the end of the bead layer obstacle and reflects off the channel bottom surface, or shortly there after due to multiple transverse wave reflections [9].

Based on the measured detonation cell size provided in Table 1, the gap above the bead layer can accommodate at least one cell for tests at an initial pressure in the range of 30-50 kPa. This is consistent with the observation that for initial pressures of 30 kPa and higher DDT occurs within the length of the bead layer, see Fig. 3a.

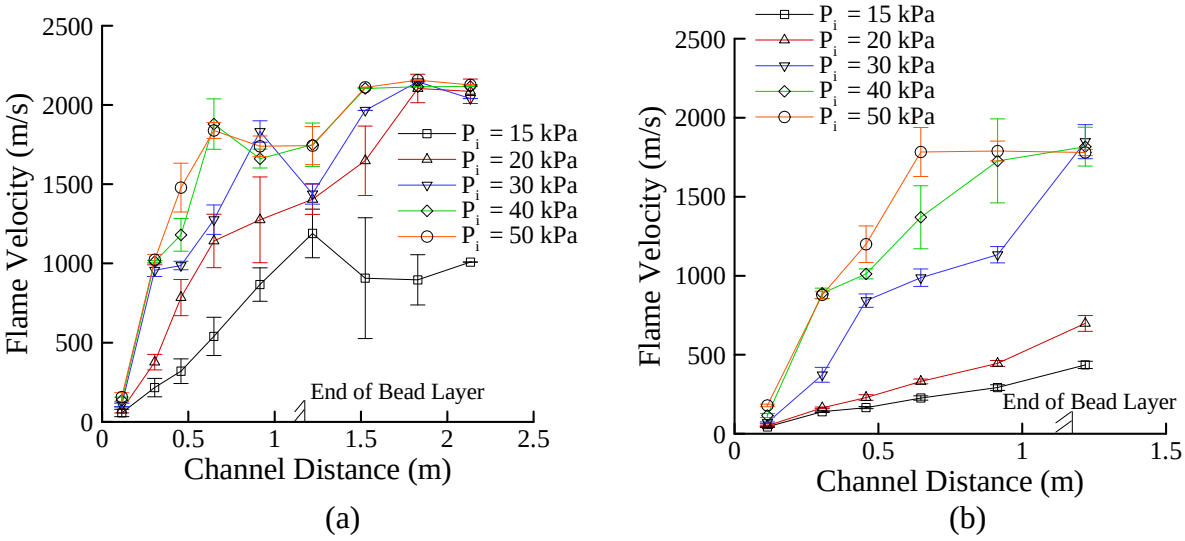

Fig 3. Axial flame velocity measured in the gap above a 43 mm nominally thick bead layer of a) 12.7 mm beads and b) 6.4 mm beads

The detonation propagates with a velocity deficit of about 200 m/s within the bead layer half of the channel and then quickly accelerates to a velocity closer to the CJ value in the smooth larger second half of the channel. For an initial pressure of 50 kPa DDT occurs very promptly with no flame velocity plateau at the speed of sound of the combustion products. For a limited number of tests a soot foil was placed on the side wall of the channel in the second half of the bead layer section. The soot foil imprint indicated that transition to detonation occurs in the gap above the bead layer. Ionization probe measurements made in the bead layer indicate a front velocity

similar to that measured in the gap. Based on the cell size measurements and the “filled tube” experiments, a self-sustained detonation wave cannot propagate in the bead layer. Therefore, the explosion front observed in the bead layer propagating at a velocity just below the CJ detonation velocity is not a self sustained detonation wave. But instead, it is believed that the detonation wave propagating in the gap drives an oblique shock wave in the bead layer that auto-ignites the mixture in the bead layer.

The same phenomena are observed for bead layer configurations with the 6.4 mm beads, see Fig. 3b for the velocity measurements. In this configuration, the ionization probes were not placed beyond the bead layer, i.e., the last flame velocity measurement was made at approximately 1.22 m away from ignition. Although the rate of flame acceleration was also observed to increase with increasing initial pressure, it was found to be lower in comparison to the larger 12.7 mm bead configuration. This is most likely due to an increase in total bead surface area associated with a smaller diameter bead that results in both an increase of energy transfer away from the reaction front along with an increase of momentum losses. Although DDT was also observed in the gap above the bead layer for tests at initial pressures of 30-50 kPa, the run-up distances were found to be larger than those observed in the 12.7 mm bead case.

The flame path through the bead layer and the free space above it are very different and thus one would expect a different velocity history. The flame velocity history through the bead layer with 12.7 mm beads was measured by ionization probes mounted on the bottom surface of the channel. The electrodes from these probes extend 15 mm into the 43 mm bead layer height, so the inferred average velocity is along the bottom one-third of the bead layer. The simultaneously measured flame time-of-arrival in the bead layer and the gap above, over the length of the bead layer section, is provided in Fig. 4 for a test at an initial pressure of 20 kPa.

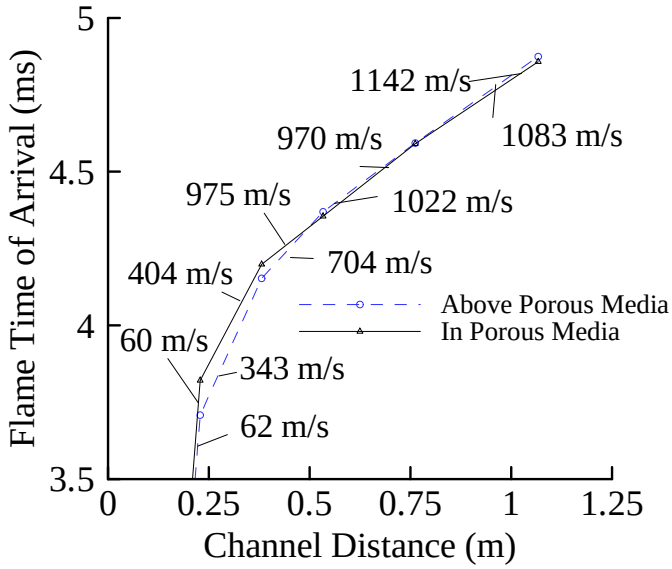

Fig 4. Time-distance plot of the flame propagation in the bead layer (12.7 mm beads) and the gap above for an initial pressure of 20 kPa

Also shown in the figure is the average axial flame velocity inferred from adjacent probe measurements. Since a good ion probe signal could not be obtained in the first instrument port location of 7.6 cm, the first time-of-arrival data point shown corresponds to the second port located at 23 cm. The velocity provided leading to the first data point is the average flame velocity from the igniter to the second ion probe. A comparison of the flame time-of-arrival at the same axial position indicates that the flame position in the gap above the bead layer is initially

ahead of the flame position in the bead layer. For example, at 23 cm the flame in the gap arrives roughly 0.12 ms before the flame in the bead layer. However, the flame velocities are not much different at that point. The flame in the bead layer then accelerates quicker than that in the gap, between 23 cm and 53 cm. At 38 cm the flame in the gap still arrives slightly before that in the bead layer despite the acceleration. At roughly 53 cm the flame time-of-arrival in both the bead layer and the gap above is the same. From this point on the flame time-of-arrivals are the same and the flame propagates at a velocity very close to the speed of sound of the combustion products. A similar behavior is observed in the tests performed at 15 kPa. For tests performed at 30-50 kPa, the flame accelerates much faster and after 23 cm the flame in the bead layer and the gap arrive at roughly the same time.

The pressure time-histories recorded simultaneously at the channel top and bottom surfaces over the length of the bead section is provided in Fig. 5. The transducer locations are given on the y-axis relative to the igniter end wall, see Fig. 1 for details on the port locations.

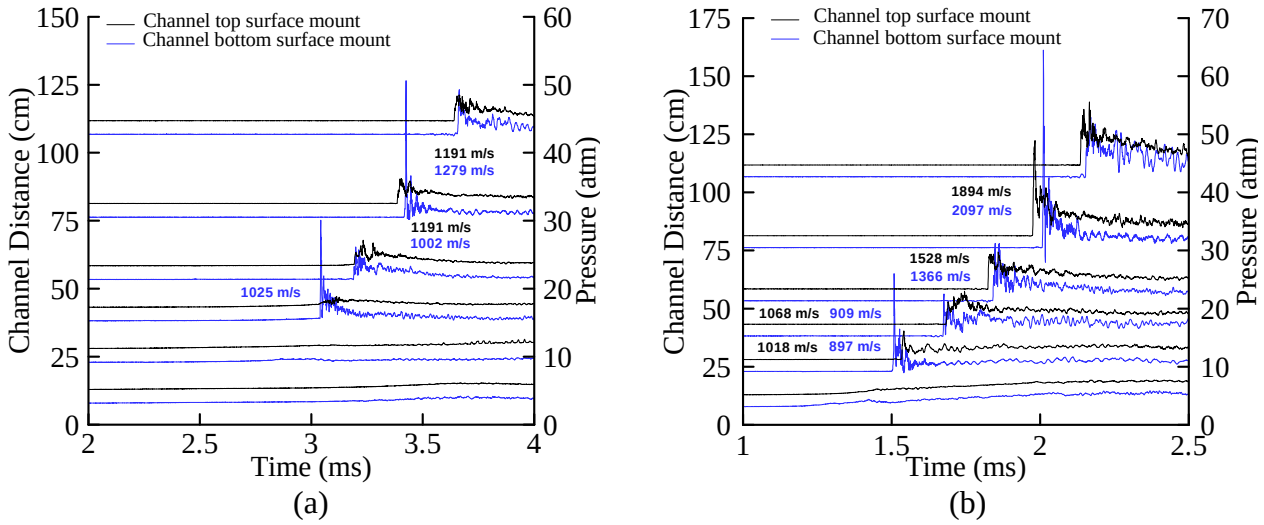

Fig 5. Pressure transients recorded at the top and bottom surfaces of the channel at different axial locations for a) initial pressure of 20 kPa, P_{CJ}= 4.82 atm, b) initial pressure of 40 kPa, P_{CJ}= 9.85 atm

For clarity the pressure traces for the transducers on the top surface are displaced vertically on the graph from the pressure traces obtained on the bottom surface. Also shown between pressure traces are the inferred shock velocities, the top/left value corresponds to the shock wave propagating in the gap. The pressure transients shown in Fig. 5a are typical of tests performed at an initial pressure of 20 kPa. At axial positions near the ignition source the pressure rises slowly as the flame velocity is significantly slower than the speed of sound of the fresh mixture. At 38 cm the pressure history recorded in the bead layer and the gap are very different. A strong shock propagates in the bead layer whereas a weak compression wave propagates in the gap. The strong shock wave forms as a result of the rapid flame acceleration in the bead layer. Based on the difference in pressure recorded at this location one would expect flow from the bead layer into the gap. At 53 cm a shock wave develops in the gap that closely follows the explosion front in the bead layer that propagates at a velocity of 1025 m/s between 38 and 53 cm. Beyond 53 cm the shock wave in the gap advances ahead of the explosion front in the bead layer and propagates at a velocity above the speed of sound in the combustion

products but well below the CJ detonation velocity. The shock velocity measurements are consistent with the flame velocity measurement provided in Fig. 4. The pressure time-histories shown in Fig. 5b were obtained from a test performed at an initial pressure of 40 kPa. At this higher initial pressure shock waves form very quickly at 23 cm in both the bead layer and the gap. As in the 20 kPa pressure measurements provided in Fig. 5a the shock wave in the bead layer initially precedes the shock wave in the gap and then advances ahead of the shock in the bead layer, in the 40 kPa test this occurs earlier at 53 cm. DDT occurs between 53 and 76 cm, beyond 76 cm the front propagates at a velocity on the order of the CJ detonation velocity.

To better understand the phenomenon, visualization of the explosion front was obtained using schlieren video with the optical module in the position shown in Fig.1. The window in the optical module is 44.4 cm long, extending between the axial positions of 8.2 cm and 52.6 cm. The maximum size of each schlieren image is restricted to a height of 7.6 cm and a length of 25.4 cm, which correspond to the channel side cut-out height and diameter of the parabolic mirror, respectively. A schlieren image of the flame propagating through the beads cannot be obtained, therefore in order to maximize the camera speed only the gap above the bead layer was visualized. This permitted the operation of the camera at 10,000 frames per second, yielding an inter-frame time of 0.1 ms. To obtain schlieren images across the full window length two experiments were performed covering the two halves of the window.

A compilation of schlieren images obtained from two experiments using 12.7 mm beads performed at an initial pressure of 30 kPa is provided in Fig. 6. The ionization probes that appear in the field of view are located at 23 cm and 38 cm from the ignition end wall. In the first frame the flame in the gap just enters the window section from the left. The flame surface appears to be relatively smooth except for a single crease that can be seen in the next frame. This crease is produced by the development of the flame past the spark plug electrode. Due to the turbulent boundary layer that develops in the unburned gas flow just above the bead layer, the lower part of the flame in the gap propagates faster than the upper part of the flame next to the top surface of the channel. The flame surface becomes more wrinkled as it accelerates approaching the first ionization probe. Starting in frame three a turbulent density interface (contact surface) emerges from the bead layer behind the flame. This corresponds to the combustion products produced behind the flame propagating in the bead layer, not visualized in Fig. 6, expanding into the gap. Since the burned gas generated in the beads is cooled by the beads it becomes visible when mixed with the hotter burned gas in the gap. This transverse flow out of the bead layer into the gap is consistent with the pressure difference noted in the simultaneous pressure measurements provided in Fig. 5.

This early time behavior can be explained by the fact that the combustion in both the bead layer and the gap is driven by turbulence produced in the unburned gas ahead of the flame. In the gap, turbulence is produced predominantly at the rough bead surface, and within the bead layer it is produced throughout by jets that form between adjacent bead cavities. The flame is continuous across the bead layer surface, therefore flame propagation in the gap will influence flame propagation in the bead layer, and visa versa. The schlieren images show that shortly after ignition, at the bead layer surface, the largely laminar flame in the gap is oblique with the leading edge at the bead layer surface, see Fig. 6. The flame shape in the bead layer during this period is not observed but one would expect a similar oblique flame only with a much shallower angle. As the combustion products expand, a flow in the unburned gas ahead of the flame is produced. There is significant resistance to this unburned gas flow in the beads, therefore expansion of the products occurs mainly into the gap propelling the flame downstream in the gap. The flame in the beads initially burns downward towards the bottom surface of the channel thus the ion probe detects the arrival of the flame in the beads at a later time. The rapid flame acceleration in the bead layer between 23 cm and 53 cm observed in Fig. 4 is a result of the oblique shape of the flame. Once the flame in the bead layer burns to the bottom surface of the channel the flame propagation becomes predominantly in the axial direction. As the turbulent

combustion in the bead layer intensifies the flame becomes more upright thus appearing, with respect to the time-of-arrival at the ionization probes, to catch up to the flame in the gap.

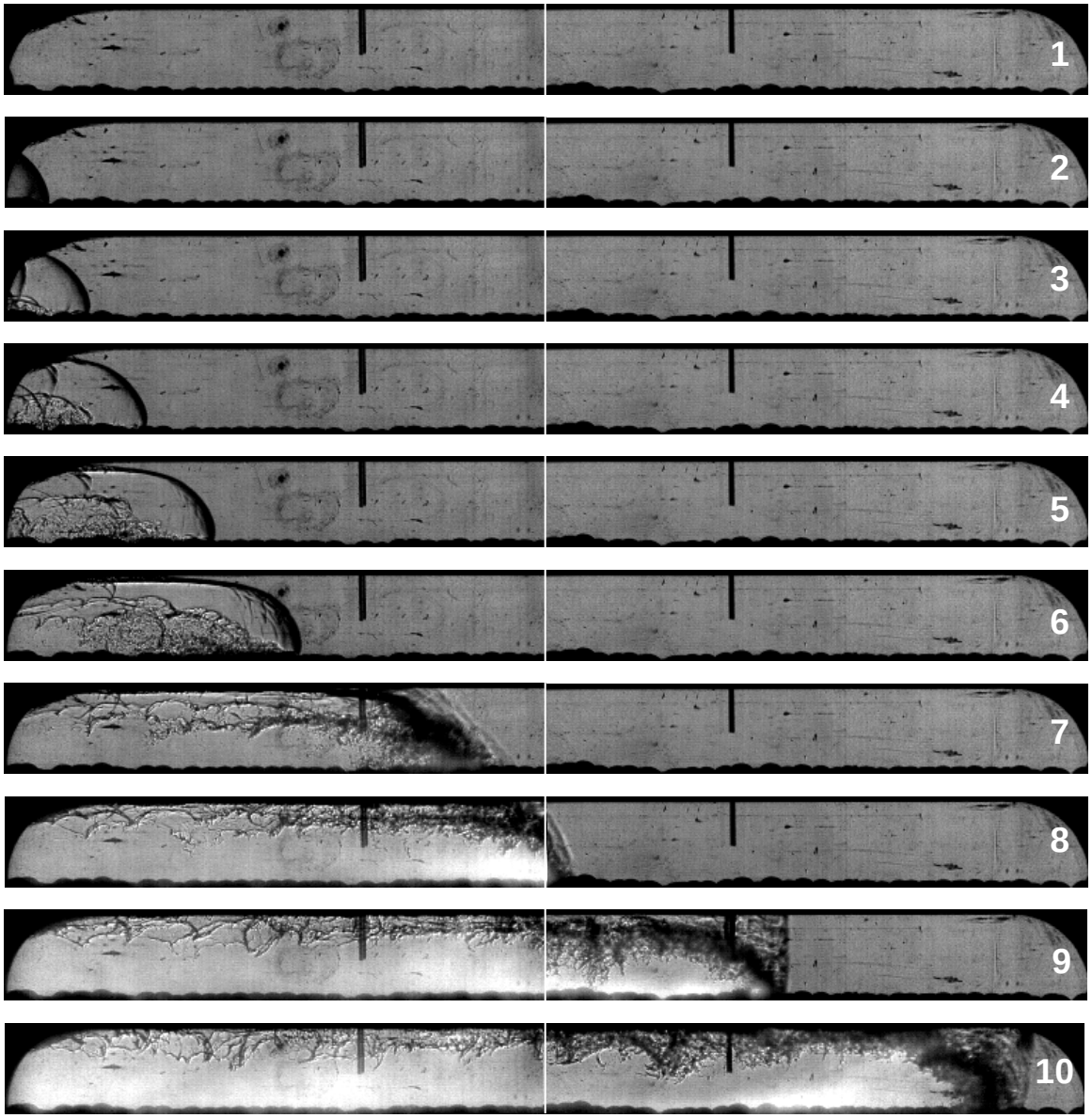

Fig 6 Explosion front propagation in the first module for initial pressure of 30 kPa. Field-of-view is 8.2 cm and 52.6 cm and the inter-frame time is 0.1 ms

In the seventh frame of Fig. 6 the flame takes on more of a wedge shape where the part of the flame immediately next to the bead layer surface surges ahead. This corresponds to the position where the flame and shock wave in the bead layer advance ahead of their counterparts in the gap, see Figs. 4 and 5. This represents a transition where the combustion in the bead layer drives the flame in the gap. The flame velocity between the sixth and seventh frame is roughly 790 m/s, and oblique compression waves appear ahead of the flame. Note, in the eighth frame the flame moves into the second half of the optical window and since the images are taken from two different experiments the location of the flame does not follow from the previous seven frames. It is apparent in the eighth frame that the shock becomes more upright and in the

ninth and tenth frame develops into a planar shock wave. The shock velocity between the eighth and ninth, and the ninth and tenth frames is 895 m/s and 980 m/s, respectively. In the last two frames there appears to be some fine structure between the flame and the shock wave that cannot be resolved in the images. This explosion front structure persists until DDT occurs in the next channel module. The framing rate of the camera is insufficient to capture the DDT event which occurs very abruptly and the subsequent detonation propagation.

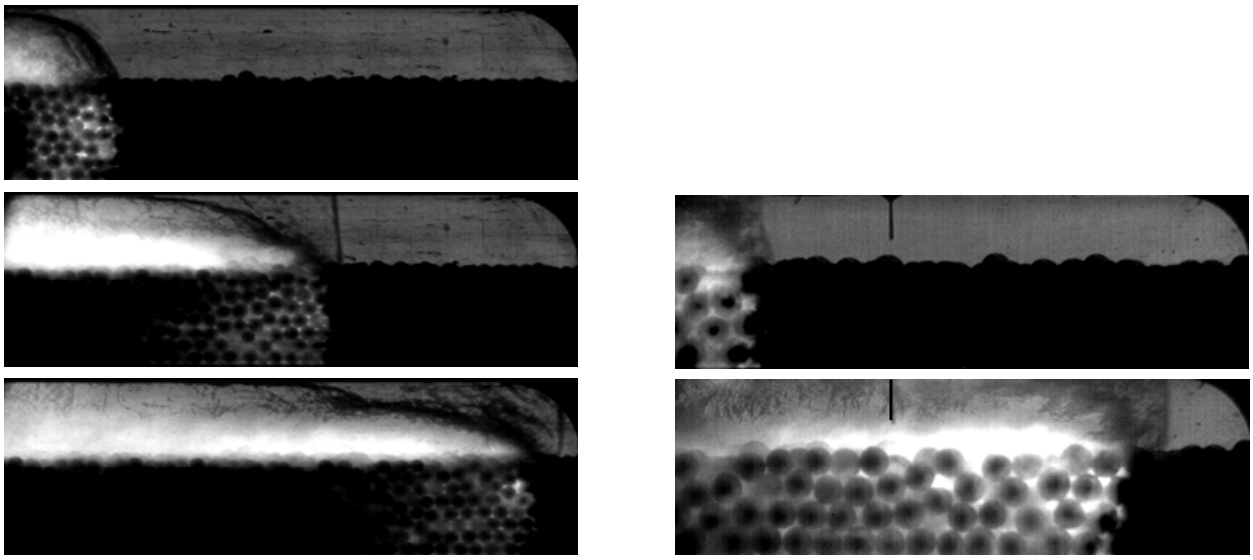

(a) (b)

Fig 7 Explosion front propagation in the second half of the window for initial pressure of 30 kPa Field-of-view is 29 cm < x < 52.6 cm for a) 6.35 mm beads (inter-frame time = 0.1 ms) and b) 12.7 mm beads (inter-frame time is 0.167 ms)

Although the schlieren system cannot detect flame propagation in the porous media due to the non-transparency of the bead layer, fast rates of combustion in the bead layer were detected in the form of light emitted between the beads when the field of view was expanded to also include the bead layer. The five Schlieren images shown in Fig. 7 are of the explosion front propagating in the second half of the optical window for an initial pressure of 30 kPa for the two bead configurations. The ionization probe viewed in the image is located at 38 cm from the ignition end wall. The average explosion front velocity during the elapsed time between frames is approximately 845 m/s for the 6.4 mm bead configuration (Fig. 7a) and 945 m/s for the 12.7 mm bead configuration (Fig. 7b). The reaction zone in the bead layer is clearly seen in the schlieren images as light emanating from between the beads along the glass surface. The source of the light is most likely the hot soot and other foreign matter that is dislodged from the beads. This finding is based on the fact that in tests using clean beads did not result in very much light emission. Based on the light emitted the reaction zone in the 6.4 mm beads extends about 10 bead diameters, whereas the reaction zone in the larger 12.7 mm beads is significantly thicker. This can be attributed to the lower products-to-bead heat transfer rate for the larger beads due to the smaller surface area. Light is also observed just above the bead layer surface behind the flame propagating in the gap providing further evidence that material is transported from the bead layer into the gap. The leading edge of the oblique flame propagating in the gap is at the same axial location as the explosion front propagating in the bead layer. Also clearly evident in the second frame for both configurations is a planar shock wave that propagates in the gap ahead of the flame in both the gap and the bead layer.

Dimpled and Smooth Solid Surface Tests

In order to determine the relative contribution of the bead layer surface roughness on flame acceleration in the gap, tests were performed by replacing the bead layer by a tightly fitting solid metal bar of similar size. A series of tests was performed with the unaltered smooth surface bar. A second series of tests was performed with the top surface of the bar roughened to simulate the condition presented by the bead layer surface. In both cases, the effect of the bead layer porosity on the combustion is removed. For the rough surface tests the effect of the surface roughness on turbulent combustion in the gap is retained. The surface roughness was produced by dimpling the surface with 6 mm deep indentations spaced at 14 mm. A ½-inch drill was used to produce the dimples. It is important to note that the dimple distribution, shown in Fig. 8, is regular compared to the more random distribution of the bead surface protrusions.

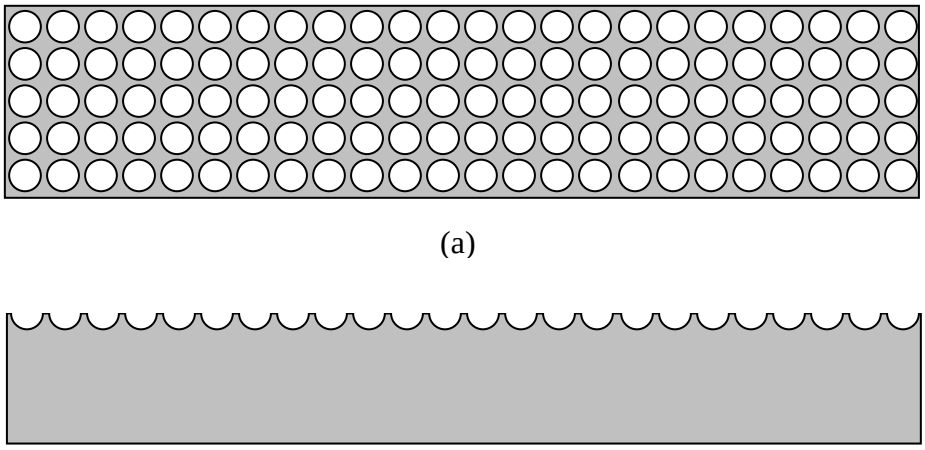

Fig 8 Schematic of dimpled metal bar; a) top view, b) cross-section view.

The flame velocity measured in the gap with the dimpled solid surface in place of the bead layer is provided in Fig. 9 along with the bead layer data from Fig. 3. In general, the initial flame acceleration to the second ionization probe, i.e., 23 cm, is stronger for the dimpled surface tests. However, beyond this point the observed flame acceleration is significantly stronger in the bead layer tests. This transition is observed further down the channel in the 15 kPa tests. For example the initial flame acceleration up to 0.4 m is stronger for the dimpled solid surface but after 0.4 m the flame acceleration is more dominant in the bead layer tests. DDT was observed with the dimpled solid surface over the initial pressure range of 30-50 kPa. This is the same DDT limit found in the bead layer tests, however, the DDT run up distance with the bead layer is much shorter.

Schlieren video taken of the flame propagating in the gap above the dimpled surface is provided in Fig. 9 for an initial pressure of 40 kPa. The photographs are taken with the optical module placed in the second channel position. The total field of view extends from 69 cm to 114 cm. The two columns of photographs come from two experiments performed at the same initial pressure. In the first frame a roughly planar shock wave enters the field of view. The shock wave propagates through the first half of the window at a constant velocity of 550 m/s. The shock wave interacts with each dimple producing a spherical wave initially centered at the dimple and then convected downstream by the planar shock flow. The shock waves produced by the five

neighboring dimples across the channel width interact and coalesce to form the quasi two-dimensional shock wave observed in the images. This shock wave propagates up towards the channel top surface where it reflects propagating back towards the dimple surface. The crisscrossing of the two families of shock waves forms a regular checkered pattern behind the planar shock wave. This checkered shock pattern is not observed in the bead layer tests, see Fig. 6. The turbulent flame just enters the field of view in the fourth frame and interacts with the transverse shock waves. It is well known that the interaction of a flame and a shock wave involves Richmeyer-Meshkov instability. This instability results in the wrinkling of the flame leading to enhanced burning rate [10, 11]. However, in the photographs the flame interaction with the transverse shock waves does not result in any clear macroscopic change in the flame surface topology. Unlike in the experiments of Thomas et al. [10], where the flame starts out laminar, in this case the flame is already fully turbulent so the effects are not as apparent. The flame is also affected by the turbulent boundary layer that grows behind the leading shock wave. The influence of the boundary layer on the flame is apparent in the photographs, as the flame propagates ahead along the bottom half of the channel. In fact the mixture near the top surface of the channel remains unburned well behind the leading edge of the flame. The relative influence of the shock waves and the boundary layer on the flame acceleration observed is not known.

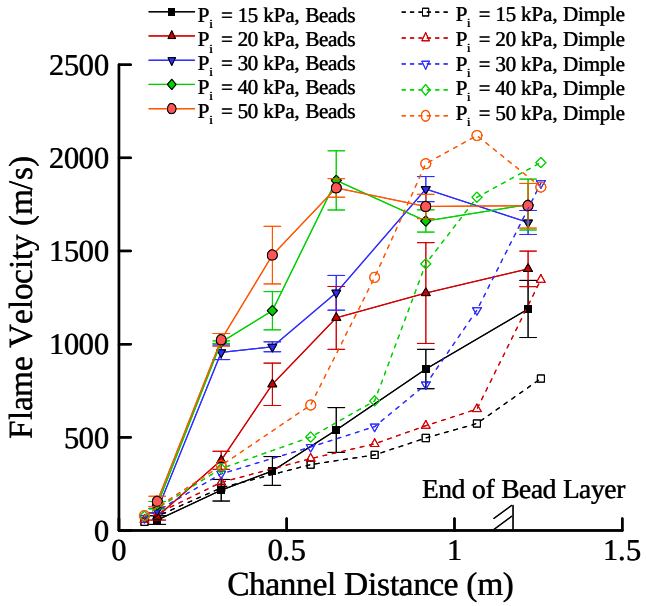

Fig 9 Flame velocity measured in the gap above the dimpled solid surface. Also shown for comparison is the flame velocity data for the bead layer tests from Fig. 3

The average flame velocity between the fourth and sixth frame in Fig. 10 is 705 m/s. This is consistent with the average flame velocity measured by the ionization probes at 68 cm and 91 cm, see the 40 kPa curve in Fig. 9. Between the fourth and sixth frames the distance between the flame and the shock wave decreases slightly indicating mild acceleration of the flame. However between the sixth and seventh frame the distance between the flame and the shock wave decreases dramatically and the flame takes on more of a wedge shape. In the eighth frame the explosion front is just at the edge of the field of view and the average flame velocity in the last two frames is about 3500 m/s. Clearly DDT occurs between the seventh and eighth frame in Fig. 10, the framing rate of the video camera is not fast enough to capture the details of

the DDT event. This is consistent with the near CJ detonation velocity measurement made between ionization probes located at 99 cm and 114 cm in Fig. 9.

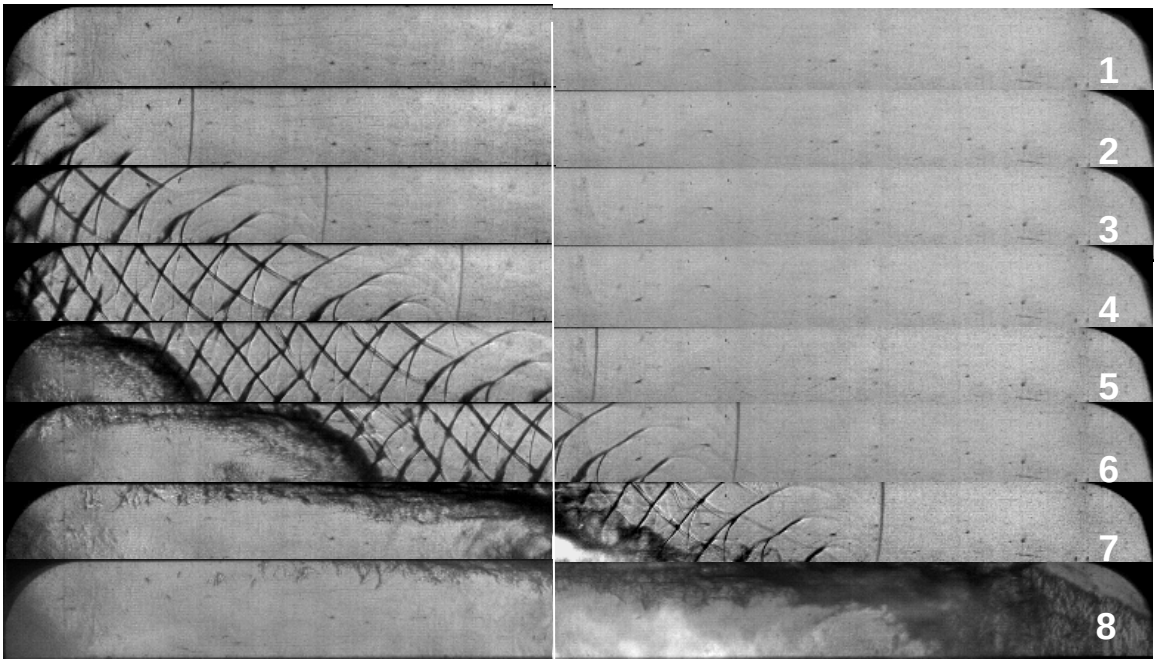

Fig 10 Flame propagation in the second channel module over the dimple surface at an initial pressure of 40 kPa. The side-by-side photographs are from two tests. The field of view extends from 69.2 cm to 113.7 cm and the inter-frame time is 100 μs

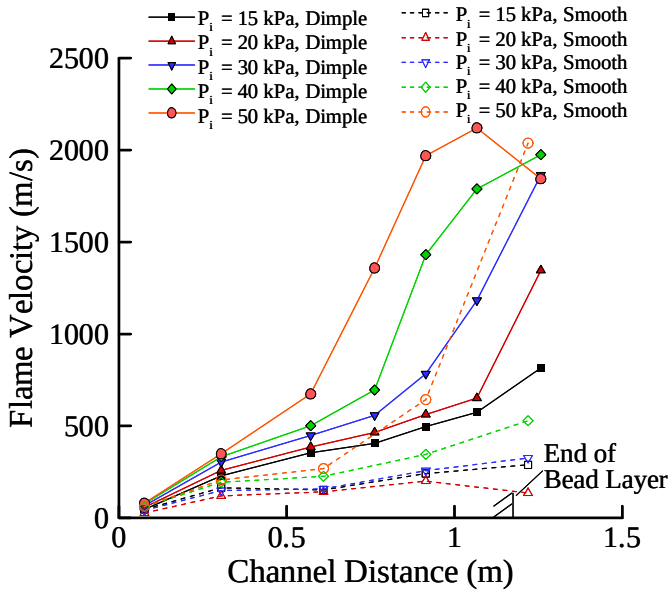

Fig 11 Flame velocity measured in the gap above the smooth solid surface. Also shown for comparison is the flame velocity data for the dimpled surface from Fig. 9

The flame velocities measured in the gap with the smooth solid surface and the dimpled surface is provided in Fig. 11. The flame acceleration measured with the smooth plate is lower

than that measured with the dimpled surface at all initial pressures. This phenomenon is well known and is the result of the rate of growth of the turbulent boundary layer ahead of the flame [12]. For the smooth plate the flame is parabolic in shape and centered within the gap, as compared to the flame over the dimpled surface which is skewed towards the dimpled surface, see Fig. 10. Between 0.3 m and 0.6 m the flame velocity does not increase very much for the smooth surface test and in general stays below 500 m/s. The exception is for 50 kPa where there is a rapid acceleration after 0.6 m of propagation. DDT occurs but this could be the result of the shock reflection after the end of the plate at 1.22 m. Since in general the flame velocity never exceeds 500 m/s compressibility effects never really play a role in the observed flame acceleration.

4 Conclusions

A comparison of the results obtained with the bead layer and the dimpled bar indicates that the combustion in the bead layer is responsible for the rapid flame acceleration observed in the bead layer tests. Essentially the turbulent combustion in the bead layer “drives” the combustion in the gap, over and above what is possible with just surface roughness. Once the flame achieves a velocity on the order of the speed of sound of the combustion products, and the gap height is larger than the mixture detonation cell size, DDT occurs in the gap. Since DDT was observed in the dimpled bar tests for the same initial pressures as that in the bead layer tests one can conclude that the DDT phenomenon is unaffected by the porosity of the bead layer. However, the stronger flame acceleration in the bead layer leads to a much shorter DDT run-up distance. The exact nature of the DDT event could not be captured in the schlieren videos due to insufficient temporal resolution. However, based on soot foil records and the shape of the flame just prior to DDT one can conclude that DDT occurs just above the bead layer surface. Future studies will look at the effect of the bead layer and gap height on the flame acceleration and DDT phenomena.

Acknowledgements

The second author would like to acknowledge discussions with Dr. Shepherd in the problem definition stage of the work. The first author was supported by the Natural Sciences and Engineering Research Council of Canada.

References

1. Babkin V.S., The problems of porous flame-arresters, Prevention of Hazardous Fires and Explosions, V.E. Zarko et al. (eds.), Kluwer Academic Publisher, Netherlands, 199-213, 1990.

2. Joo P., Duncan K., and Ciccarelli G., Flame Quenching Performance of Ceramic Foam, Combustion Science and Technology, 178(10-11):1755, 2006.

3. Hlouschko S. and Ciccarelli G., Proceedings of the 21st International Colloquium on the Dynamics of Explosions and Reactive Systems, Futuroscope, France, 2007.

4. Babkin V.S., Korzhavin A.A., and Bunev V.A., Propagation of premixed gaseous explosion flames in porous media, Combustion and Flame, 87:182-190, 1991.

5. Pinaev A.V., Combustion modes and flame propagation criteria for an encumbered space, Combustion, Explosion, and Shock Waves 30(4):454-461, 1994.

6. Makris A., Shafique H., Lee J.H., and Knystautas R., Influence of mixture sensitivity and pore size on detonation velocities in porous media, Shock Waves, 5:589-95, 1995.

7. Peraldi O., Knystautas R., and Lee J.H., Criteria for transition to detonation in tubes, Proceedings of the Combustion Institute, 21:1629-1637, 1986.

8. Mihalik T.A., Lee J.H., Continillo G. and Marra F.S., Quenching Mechanisms of Gaseous Hydrocarbon-Air Flames in Packed Beds, Proceedings of the 18th International Colloquium on the Dynamics of Explosions and Reactive Systems, Seattle, U.S., 2001.

9. Pantow E.G., Fischer M, Kratzel Th., Decoupling and recoupling of detonation waves associated with sudden expansion, Shock Waves 6: 131-137, 1996.

10. Thomas G.O., Sands C.J., Brambrey R.J. and Jones S.A., Experimental Observations of the Onset of Turbulent Combustion Following Shock-Flame Interaction, Proceedings of the 16th International Colloquium on the Dynamics of Explosions and Reactive Systems, Cracow, Poland, 1997.

11. Khokhlov A.M., Oran E.S. and Thomas G.O., Numerical Simulation of Deflagration-to-Detonation Transition: The Role of Shock-Flame Interactions in Turbulent Flames, Combustion and Flame, 117**:** 323-339, 1999.

12. M. Kuznetsov, I. Matsukov, V. Alekseev, W. Breitung, S. Dorofeev, Proceedings of the 20th International Colloquium on the Dynamics of Explosions and Reactive Systems, Montreal, Canada, 2005.